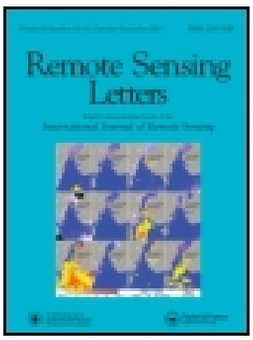

Remote Sensing Letters

ISSN: 2150-704X (Print) 2150-7058 (Online) Journal homepage: http://www.tandfonline.com/loi/trsl20

A method to detect earthquake-collapsed buildings from high-resolution satellite images

Wenzhong Shi & Ming Hao

To cite this article: Wenzhong Shi & Ming Hao (2013) A method to detect earthquake-collapsed buildings from high-resolution satellite images, Remote Sensing Letters, 4:12, 1166-1175, DOI: 10.1080/2150704X.2013.858839

To link to this article: http://dx.doi.org/10.1080/2150704X.2013.858839

Remote Sensing Letters, 2013
Vol. 4, No. 12, 1166–1175, http://dx.doi.org/10.1080/2150704X.2013.858839

Taylor & Francis
Taylor & Francis Group

A method to detect earthquake-collapsed buildings from high-resolution satellite images

WENZHONG SHI† and MING HAO*‡
†Joint Research Laboratory on Spatial Information, The Hong Kong Polytechnic University and Wuhan University, Wuhan and Hong Kong, China
‡Jiangsu Key Laboratory of Resources and Environmental Information Engineering, China University of Mining and Technology, Xuzhou, China

(*Received 12 April 2013; accepted 17 October 2013*)

A method is proposed to detect collapsed buildings induced by earthquakes. The method computes quantitative indices of the spectral responses for the city plan objects (buildings), assuming that a building was collapsed if the spectral response is sufficiently heterogeneous. First, the pre-earthquake boundaries of buildings stored in the geographic information system (GIS) vector data are used as a reference for determining the extent of each building in the post-image. Second, an improved active contour model is implemented to extract those homogeneous regions in the building boundaries on the post-earthquake image. Third, the shape similarity index (SSI) between the extracted homogeneous region and the corresponding pre-building boundary is calculated, and the area ratio index (ARI) between the extracted homogeneous pixel areas and the true reference pixel areas is calculated. Finally, the *k*-means clustering method is implemented to partition buildings into collapsed and undamaged sections based on the SSI and ARI. The experimental results indicate the strong robustness and high effectiveness of the proposed method. It is worth noting that a threshold is not needed to determine whether buildings are collapsed. The method quickly and accurately provides information on collapsed buildings.

1. Introduction

Strong magnitude (high on the Richter scale) and shallow earthquakes have a severe impact on cities and urban infrastructure. Near real-time mapping of the earthquake's impact on urban infrastructure is critical for civil protection purposes. With the development of spatial information technology, post-earthquake remotely sensed images have become an important data source for the detection and assessment of hard-hit areas (Turker and Cetinkaya 2005). A number of studies have been performed using such remotely sensed images to detect earthquake-damaged buildings.

The building height information pre- and post-earthquake is used based on digital elevation models (DEMs) to detect damaged buildings (Gupta *et al.* 1994, Turker and Cetinkaya 2005, Rehor 2007). An image differencing change detection technique has also been used to detect earthquake damage (Gupta *et al.* 1994). Saraf *et al.* (2002) used the pseudo-colour transform technique (PTC) to map landslides and damaged houses caused by earthquakes. Alvanitopoulos *et al.* (2010) identified damaged buildings by designing classification models based on artificial neural

*Corresponding author. Email: haomingcumt@gmail.com

networks and neuro-fuzzy systems. Very high-resolution synthetic aperture radar (SAR) images have also been used to detect building damage, along with optical images in some studies (Matsuoka and Yamazaki 2004, Gamba *et al.* 2007, Chini *et al.* 2009, Brunner *et al.* 2010, Dong *et al.* 2011). Three-dimensional (3D) geometric changes using pre- and post-seismic IKONOS stereo image pairs help to detect collapsed buildings in an earthquake (Tong *et al.* 2012). Additionally, geographic information system (GIS) data can provide building location information and improve the accuracy of damaged building detection (Altan *et al.* 2001, Turker and San 2004, Turker and Sumer 2008, Sahar *et al.* 2010). In the present study, GIS data were used to provide building boundaries.

Normally, in a high-resolution remotely sensed image, undamaged buildings appear to be relatively homogeneous, whereas the grey values of collapsed buildings highlight heterogeneous areas. The shapes and areas of the homogeneous regions of an undamaged building should be same as the initial shape and area stored in the pre-event GIS. Based on this understanding, a method is proposed to detect earthquake-collapsed buildings, utilizing a post-event satellite image and building boundary vectors available from the pre-event GIS data.

2. Methodology

The proposed method consists of three steps: (1) pre-processing of the GIS data and the high-resolution satellite image, (2) extracting the homogeneous regions in the initial building boundaries from the remotely sensed image using an improved active contour model and (3) determining whether buildings are collapsed based on the shape similarity index (SSI) and area ratio index (ARI) measurements by clustering.

The pre-earthquake building boundaries are used to extract the building area image from the post-earthquake satellite image, as presented in figure 1. The red solid line polygon is the building boundary, and the blue polygon is the bounding rectangle of the building boundary used to extract the building area image. The building area images are processed one-by-one by the improved active contour model.

2.1 *Improved active contour model*

The active contour model (snake model) (Kass *et al.* 1988) is an energy-minimizing curve that moves within the image domain to capture a target object. The curve's motion is driven by a combination of internal and external forces. It achieves a closed contour when a minimal energy state is reached (i.e., the pixels inside and outside the contour are mostly homogeneous). The active contour model proposed by Chan and Vese (2001) is one of most widely used active contour models. The Chan–Vese model is adopted for this

(*a*) (*b*)

Figure 1. Input data of the improved active contour model. (*a*) Undamaged and (*b*) collapsed buildings.

study because of its advantages in the implicit handling of topological changes, extraction of objects without noticeable edges and low sensitivity to noise.

The energy function of the initial model for multiband images is given by (Chan and Vese 2001, Ahmadi *et al.* 2010)

$$E_0 = vL(C) + \mu A(I(C)) + \lambda_1 \sum_{b=1}^{3} \int_{I(C)} |u_b(x,y) - c_{1b}|^2 \mathrm{d}x\mathrm{d}y + \lambda_2 \sum_{b=1}^{3} \int_{O(C)} |u_b(x,y) - c_{2b}|^2 \mathrm{d}x\mathrm{d}y \quad (1)$$

where $\mu \geq 0$, $v \geq 0$ and λ_1, $\lambda_2 > 0$ are fixed parameters, C is the evolving curve, $I(C)$ represents the area inside the evolving curve, $O(C)$ represents the area outside the evolving curve, $L(C)$ denotes the length of the evolving curve, $A(I(C))$ denotes the area surrounded by the evolving curve, b is the band number, $u_b(x,y)$ is the value of pixel (x,y) of the corresponding image band and c_{1b} and c_{2b} are the mean grey values of all the pixels inside and outside the curve C, respectively, for the corresponding band. The term $\int_{I(C)} |u_b(x,y) - c_{1b}|^2 \mathrm{d}x\mathrm{d}y$ is the sum of the differences between the pixel grey value inside the contour and the corresponding mean value for band b. Similarly, the term $\int_{O(C)} |u_b(x,y) - c_{2b}|^2 \mathrm{d}x\mathrm{d}y$ is the sum of the differences between the pixel grey value outside the contour and corresponding mean value for the band b. The contour then evolves to fit the edges of objects by forcing equation (1) to reach a minimum value. Finally, the image is segmented into two parts, each with homogeneous pixels.

The Chan–Vese model only segments images of simple objects, and for complex remotely sensed images, a multiphase framework is needed (Bazi *et al.* 2010). To partly overcome this problem and make it appropriate to extract homogeneous regions from building area images, a term is added to equation (1). Existing techniques are used to extract the urban building boundary (Ahmadi *et al.* 2010). The improved equation is rewritten as

$$E = E_0 + \lambda_3 \sum_{b=1}^{3} \int_{I(C)} |u_b(x,y) - s_b|^2 \mathrm{d}x\mathrm{d}y \quad (2)$$

where $\lambda_3 > 0$ is a constant coefficient, $\sum_{b=1}^{3} \int_{I(C)} |u_b(x,y) - s_b|^2 \mathrm{d}x\mathrm{d}y$ is the sum of the grey value variance between the samples and pixels at building boundaries, and s_b is the grey value of building samples corresponding to band b. Fifty samples are selected randomly for building boundaries. Fifteen samples that deviated significantly from the average of all samples are removed to obtain a robust building sample. The remaining 35 samples are used, and their average is calculated as the final sample value, which is considered as a statistical result. As mentioned in section 1, if the building is undamaged, the final sample represents the general grey value of the building roof and is helpful for extracting completely homogenous building roofs. In contrast, the collapsed building is only partly extracted.

The level set method (Osher and Sethian 1988) is used to calculate the energy function. More details on the Chan–Vese active contour model can be found in Chan and Vese (2001). In this study, we generally choose the parameters as follows: $\lambda_1 = \lambda_2 = \lambda_3 = 1$, $\mu = 0$

and the time step of Chan–Vese model $\Delta t = 0.1$, as recommended by Chan and Vese (2001). The length parameter (v) has a scaling role. To detect many objects of any size, v should be small, whereas v must be larger to detect only larger objects. Because the Chan–Vese model is used to detect homogenous areas of collapsed buildings, including many small regions, the parameter v is set to a small value (i.e., 0.2).

2.2 *Determining whether buildings are damaged*

The homogeneous regions within building boundaries are extracted from the building area images by the improved Chan–Vese model. Thus, the SSI and ARI can be calculated based on the extracted homogeneous regions.

2.2.1 Shape similarity index. The SSI indicates the degree of similarity between the shape of the extracted homogenous region of a building and the corresponding shape stored in the GIS data. The method proposed by Ling and Jacobs (2007) based on shape context was used to calculate the SSI values. The details are provided in the following section.

First, the isolated pixels belonging to the homogeneous regions are removed, and n sample points are selected on the edge of the homogeneous regions to represent the shape of the homogeneous regions.

Second, the shape context is built for all sample points. As shown in figure 2(*a*), the shortest path between boundary point p and another point q defined with the inner-distance is recorded as $d(p,q)$. The angle between the contour tangent at p and the direction of the shortest path $d(p,q)$ is defined as the inner-angle, denoted as $\theta(p,q)$. The $d(p,q)$ and $\theta(p,q)$ together are viewed as a vector. Thus, n–1 vectors, composed of the inner-distance and inner-angle, can be generated for other n–1 sample points. Third, the shape context histograms are generated for the n–1 vectors. The inner-distance and inner-angle are divided into n_d and n_θ bins, respectively, by splitting their magnitudes. For a point p on the shape, the histogram h for n–1 vectors relative to the remaining n–1 points is computed as follows:

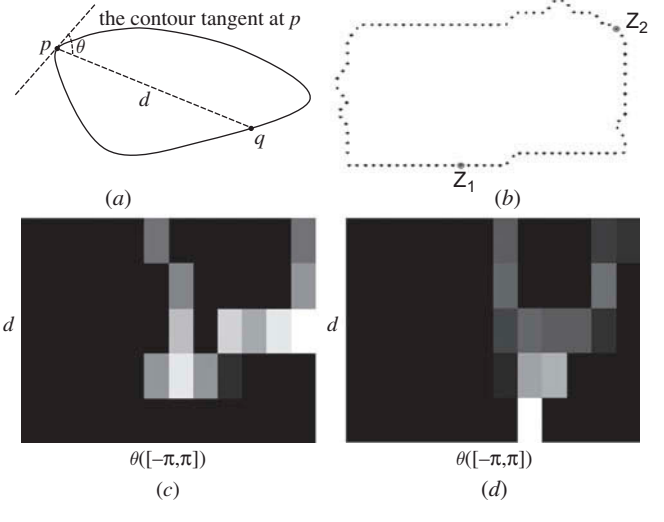

Figure 2. Establishment of shape context histograms. (*a*) Inner-distance and inner-angle; (*b*) sample points on the boundary; (*c*) and (*d*) shape context histograms of Z_1 and Z_2, respectively.

$$h(k) = N\{p \neq q_i, (p - q_i) \in \text{bin } k\} \tag{3}$$

where q_i is the i-th boundary point, $k \in \{1,2,\ldots,K\}$, $K = n_d n_\theta$ and N denote the number of vectors falling into the bin k. Figure 2(*b*) displays the extracted shape of a building and figures 2(*c*) and (*d*) present the histograms of points Z_1 and Z_2, respectively, in figure 2(*b*). Therefore, n histograms are computed corresponding to n sample points, and they are utilized to calculate the similarity between the two shapes.

Finally, the SSI values are computed by minimizing the cost of matching between the extracted homogenous shape and corresponding building shape stored in the GIS data, considering the points p_i and q_j on the first and second shapes, respectively. C_{ij} denotes the cost of matching the two points. The shape contexts are distributions represented as histograms (figure 2), and the cost is measured using the χ^2 test statistic (Belongie *et al.* 2002):

$$C_{ij} = C(p_i, q_j) = \frac{1}{2}\sum_{k=1}^{K}\frac{[h_i(k) - h_j(k)]^2}{h_i(k) + h_j(k)} \tag{4}$$

where $h_i(k)$ and $h_j(k)$ are the shape context histograms of p_i and q_j, respectively, and K is the number of histogram bins. The matching s should minimize the match cost $H(s)$ between the two shapes for n points. $H(s)$ is defined as

$$H(s) = \sum_{1 \leq i \leq n} C(p_i, q_{s(i)}). \tag{5}$$

Dynamic programming is used to solve the matching problem, and the matching cost $H(s)$ is used to measure the similarity between the shapes. Further details can be found in Ling and Jacobs (2007).

Generally, a larger n will obtain more accurate results with less efficiency; $n = 100$ was used in this experiment. Typical settings for the bin numbers are $n_d = 5$ and $n_\theta = 12$ (Ling and Jacobs 2007), which are sufficient to obtain favourable histograms. Hence, the bin numbers are set to the typical values.

2.2.2 Area ratio index. The ARI denotes the ratio of the total number of pixels within the homogeneous area on the building area images and the total number of pixels falling within the corresponding building boundary stored in the GIS. The number of pixels in the extracted homogeneous area of the ith building is recorded as a_i, and the number of pixels in the corresponding building A_i can be acquired from the GIS data. The ARI value r_i is calculated as follows:

$$r_i = a_i / A_i. \tag{6}$$

2.2.3 Clustering based on the SSI and ARI. It is difficult to identify collapsed buildings by setting thresholds to the SSI and ARI because different thresholds critically affect detection results. Given this fact, the k-means clustering method is used to determine damaged buildings based on the SSI and ARI where thresholds are not required. The k-means clustering aims to partition observations into k clusters where each observation belongs to the cluster with the nearest mean.

Given the observations $\mathbf{X}=\{\boldsymbol{x}_1, \boldsymbol{x}_2, ..., \boldsymbol{x}_n\}$, where each observation means a vector consists of ARI and SSI of a building, and we know that they fall into two clusters $T = \{T_1, T_2\}$. The observations are partitioned into two clusters by minimizing the objective function:

$$J = \sum_{i=1}^{2} \sum_{\boldsymbol{x}_j \in T_i} \left\| \boldsymbol{x}_j - \boldsymbol{m}_i \right\|^2 \tag{7}$$

where $\boldsymbol{m}_i$ is the mean of the observations in cluster i. Further details on this method can be found in Bishop (2006).

The k-means cluster method is then used to partition buildings into collapsed and undamaged parts by minimizing equation (7).

3. Experimental results and discussion

The Yushu county of China experienced an earthquake of magnitude 7.1 on the Richter scale on 14 April 2010. The study area is one of the most strongly impacted by the earthquake. The data were obtained by QuickBird on 15 April 2010 with a resolution of 0.61 m, and the fusion image prepared from panchromatic and multispectral images was used to detect collapsed buildings. This image (400 × 466 pixels), cropped to the study area, is presented in figure 3(*a*), which is a fusion of panchromatic and multispectral images. Normally, the boundaries of buildings should be obtained from GIS data; however, it was difficult to obtain the GIS data in this study. Hence, the GIS polygon was digitized from QuickBird imagery acquired in May 2009. First, the pre- and post-earthquake images were assigned the same latitude/longitude reference system (World Geodetic System 1984 (WGS 84)) and were registered by an image-to-image registration in The Environment for Visualizing Images (ENVI). Both images were registered at an accuracy of 0.2 pixels using a polynomial first degree polynomial. The vector corresponding to the pre-earthquake city plan (polygon buildings) mapped at a scale of 1:5000 was digitized from a pre-earthquake satellite image and projected to the latitude/longitude reference system WGS 84, as shown in figure 3(*b*). The post-earthquake image with a spatial resolution of 0.61 m, along with the building boundaries, was used to detect collapsed buildings. The ground reference, whether the building is actually collapsed, was produced by visual interpretation and used to assess the accuracy of detected results.

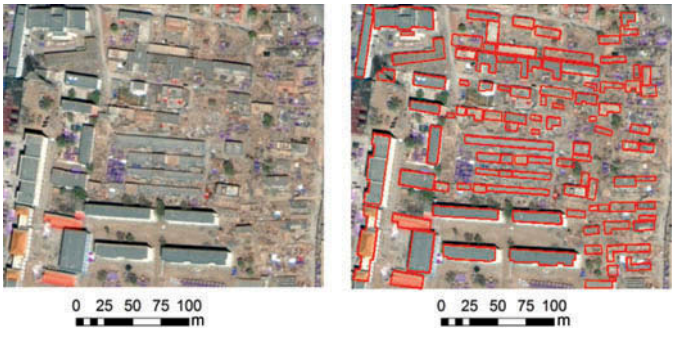

(*a*) (*b*)

Figure 3. (*a*) High-resolution remotely sensed image of the study area captured by QuickBird and (*b*) building boundaries generated by digitizing pre-earthquake high-resolution image (the centre coordinate: 32° 59′ N, 97° 0′ E).

After pre-processing and registration between the QuickBird image and the pre-event vector data, the improved active contour model was implemented to extract the homogeneous regions of buildings. The extracted homogeneous regions are shown in figure 4(*a*). Undamaged buildings with a roof of a single colour were extracted as almost completely homogenous regions, such as part 1 of figure 4(*a*). For the undamaged buildings with roofs of more than one colour, this method does not work well, as shown by part 2 of figure 4(*a*). For collapsed buildings, the homogenous regions were extracted dispersedly (e.g., parts 3–5), which validates the main hypothesis that collapsed buildings display heterogeneous regions while undamaged buildings display relatively large homogeneous regions.

The SSI and ARI values were then calculated (using the parameters discussed in section 2.3.1) between the extracted homogeneous regions and building boundaries stored in the GIS data. The *k*-means method was implemented to partition the buildings into damaged and undamaged clusters based on the SSI and ARI values. The buildings are shown as points in the coordinate system where the ARI values are

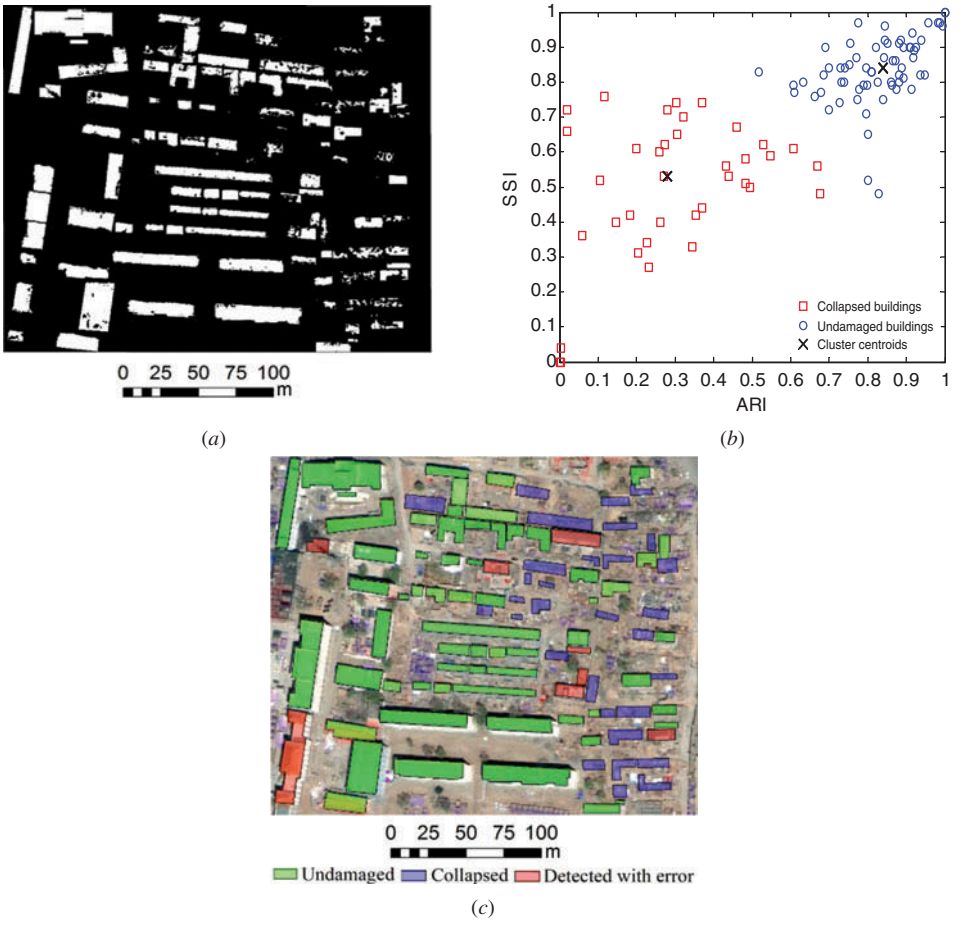

Figure 4. (*a*) Extracted homogeneous regions (bright parts) by improved active contour model; (*b*) clustering result based on SSI and ARI of buildings and (*c*) detected result for collapsed buildings.

plotted on the x-axis and the SSI values on the y-axis. The clustering result of the buildings is depicted in figure 4(b), in which the red rectangles are collapsed buildings and the blue circles denote undamaged buildings. Additionally, the centroids of the clusters were (0.28, 0.53) and (0.84, 0.84) (figure 4(b)).

The results are shown in figure 4(c), in which the collapsed and undamaged buildings detected correctly are displayed in blue and green, respectively, and red denotes detected errors. Of all 102 buildings, 94 buildings were classified correctly, providing an overall accuracy of 92.16%. Sixty-three undamaged buildings were identified correctly out of a total of 69 buildings, resulting in an accuracy of 91.30%. Thirty-one collapsed buildings were detected correctly out of 33, resulting in an accuracy of 93.94%. The detailed accuracy of detected results is depicted based on objects in table 1.

Additionally, an approach proposed by Turker and Sumer (2008) called the watershed segmentation of the post-event aerial images (WSPAI) was implemented for a comparison. The buffer boundary and depth were set to 6 and 3 pixels, respectively, and the threshold ranged from 20% to 50% at 10% intervals. As shown in figure 5, the accuracy increased with the increasing value of threshold and reached a maximum at the threshold of 30%. The accuracy was observed to decrease until the threshold value of 80%. The determination of the optimal threshold is very important for identifying collapsed buildings. In contrast to WSPAI, a threshold is not needed for the detection of collapsed buildings in the proposed work, which enhances the robustness of the detection results.

The proposed method has several advantages. The first is that the assessment was performed using known buildings compared with traditional studies lacking GIS data, which reduces errors in extracting buildings. The detected results cannot be affected by other buildings and objects. The second advantage is that the method is better suited for the identification of collapsed buildings. When buildings are seriously damaged, the extracted homogeneous region is more cracked and more easily identified. People buried within these collapsed buildings can be reached more rapidly, making rescues more likely. Moreover, a threshold is not needed in the proposed method for the identification of a collapsed building. The k-means clustering method is used to determine collapsed buildings by grouping them into two classes based on the SSI and ARI, thus avoiding the use of an uncertain threshold, like those used in the traditional methods (i.e., Kosugi *et al.* 2004, Turker and Sumer 2008).

This approach, however, does have some limitations that need to be reduced or overcome. An up-to-date pre-earthquake GIS database should be available for accurately extracting building boundaries. Furthermore, damaged buildings could not be properly detected in the following cases: (1) the building is damaged but still stands beneath a homogeneous undamaged roof, (2) the building is covered by a shadow cast by other buildings or trees nearby and (3) the building has a roof with multiple colours. Further research needs to be performed to overcome these drawbacks.

Table 1. Error matrix of detected results.

	Reference			
Analysed data	No. of collapsed buildings	No. of undamaged buildings	Total	Accuracy (%)
Collapsed buildings	31	6	37	93.94
Undamaged buildings	2	63	65	91.30
Total	33	69	102	92.16

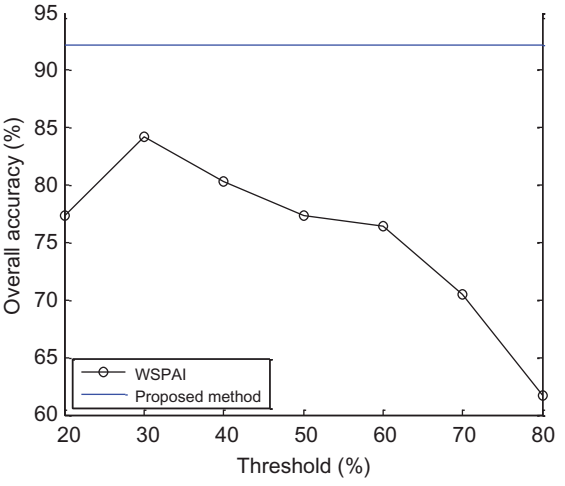

Figure 5. Comparison between the proposed method and WSPAI.

4. Conclusions

In this research, a method of detecting buildings that collapse due to earthquakes that is based on the use of pre-earthquake GIS data and post-earthquake high-resolution satellite images was developed. The improved active contour model was utilized to extract homogenous regions from post-earthquake satellite images. The SSI and ARI were calculated from the extracted homogenous regions, and *k*-means was implemented to identify collapsed buildings by clustering in the SSI and ARI. The results of the experiments conducted to test the proposed method were promising, providing an overall accuracy of 92.16%. In contrast to other methods of detecting damaged buildings, a threshold is not needed in the proposed method to determine damaged buildings. Quick and accurate information is provided by this method for rescue. However, some challenges, such as damaged buildings with complete roofs, shadows and roofs with multiple colours, require further research.

Funding

The work presented in this letter is supported by Ministry of Science and Technology of China [Project No.: 2012BAJ15B04].

References

Ahmadi, S., Valadan Zoej, M.J., Ebad, H. and Moghaddam, H.A., 2010, Automatic urban building boundary extraction from high resolution aerial images using an innovative model of active contours. *International Journal of Applied Earth Observation and Geoinformation*, **12**, pp. 150–157.

Altan, O., Toz, G., Kulur, S., Seker, D., Volz, S., Fritsch, D. and Sester, M., 2001, Photogrammetry and geographic information systems for quick assessment, documentation and analysis of earthquakes. *ISPRS Journal of Photogrammetry and Remote Sensing*, **55**, pp. 359–372.

Alvanitopoulos, P.F., Andreadis, I. and Elenas, A., 2010, Neuro-fuzzy techniques for the classification of earthquake damages in buildings. *Measurement*, **43**, pp. 797–809.

Bazi, Y., Melgani, F. and Al-Sharari, H.D., 2010, Unsupervised change detection in multispectral remotely sensed imagery with level set methods. *IEEE Transactions on Geoscience and Remote Sensing*, **48**, pp. 3178–3187.

BELONGIE, S., MALIK, J. and PUZICHA, J., 2002, Shape matching and object recognition using shape context. *IEEE Transactions on Pattern Analysis and Machine Intelligence*, **24**, pp. 509–522.

BISHOP, C.M., 2006, *Pattern Recognition and Machine Learning*, pp. 424–430 (New York: Springer).

BRUNNER, D., LEMOINE, G. and BRUZZONE, L., 2010, Earthquake damage assessment of buildings using VHR optical and SAR image. *IEEE Transactions on Geoscience and Remote Sensing*, **48**, pp. 2403–2420.

CHAN, T.F. and VESE, L.A., 2001, Active contours without edges. *IEEE Transaction on Image Processing*, **10**, pp. 266–277.

CHINI, M., PIERDICCA, N. and EMERY, W.J., 2009, Exploiting SAR and VHR optical images to quantify damage caused by the 2003 Bam earthquake. *IEEE Transactions on Geoscience and Remote Sensing*, **47**, pp. 145–152.

DONG, Y., LI, Q., DOU, A. and WANG, X., 2011, Extracting damages caused by the 2008 Ms 8.0 Wenchuan earthquake from SAR remote sensing data. *Journal of Asian Earth Sciences*, **40**, pp. 907–914.

GAMBA, P., DELL'ACQUA, F. and TRIANNI, G., 2007, Rapid damage detection in the Bam area using multitemporal SAR and exploiting ancillary data. *IEEE Transactions on Geoscience and Remote Sensing*, **45**, pp. 1582–1589.

GUPTA, R.P., SARAF, A.K., SAXENA, P. and CHANDER, R., 1994, IRS detection of surface effects of the Uttarkashi earthquake of 20 October 1991, Himalaya. *International Journal of Remote Sensing*, **15**, pp. 2153–2156.

KASS, M., WITKIN, A. and TERZOPOULOS, D., 1988, Snakes: active contour models. *International Journal of Computer*, **1**, pp. 321–331.

KOSUGI, Y., SAKAMOTO, M., FUKUNISHI, M., LU, W., DOIHARA, T. and KAKUMOTO, S., 2004, Urban change detection related to earthquakes using an adaptive nonlinear mapping of high-resolution images. *IEEE Geoscience and Remote Sensing Letters*, **1**, pp. 152–156.

LING, H. and JACOBS, D.W., 2007, Shape classification using the inner-distance. *IEEE Transaction on Pattern Analysis and Machine Intelligence*, **29**, pp. 286–299.

MATSUOKA, M. and YAMAZAKI, F., 2004, Use of satellite SAR intensity image for detecting building areas damaged due to earthquakes. *Earthquake Spectra*, **20**, pp. 975–994.

OSHER, S. and SETHIAN, J.A., 1988, Fronts propagating with curvature-dependent speed: algorithms based on Hamilton-Jacobi formulation. *Journal of Computational Physics*, **79**, pp. 12–49.

REHOR, M., 2007, Classification of building damages based on laser scanning data. In *Proceedings of the ISPRS Workshop 'Laser Scanning 2007 and SilviLaser 2007'*, 12–14 September 2007, Espoo, pp. 326–331.

SAHAR, L., MUTHUKUMAR, S. and FRENCH, S.P., 2010, Using aerial image and GIS in automated building footprint extraction and shape recognition for earthquake risk assessment of urban inventories. *IEEE Transactions on Geoscience and Remote Sensing*, **48**, pp. 3511–3520.

SARAF, A.K., SINVHAL, A., SINVHAL, H., GHOSH, P. and SARMA, P., 2002, Satellite data reveals 26 January 2001 Kutch earthquake-induced ground changes and appearance of water bodies. *International Journal of Remote Sensing*, **23**, pp. 1749–1756.

TONG, X., HONG, Z., LIU, S., ZHANG, X., XIE, H., LI, Z., YANG, S., WANG, W. and BAO, F., 2012, Building-damage detection using pre-and post-seismic high-resolution satellite stereo imagery: a case study of the May 2008 Wenchuan earthquake. *ISPRS Journal of Photogrammetry and Remote Sensing*, **68**, pp. 13–27.

TURKER, M. and CETINKAYA, B., 2005, Automatic detection of earthquake-damaged buildings using DEMs created from pre- and post-earthquake stereo aerial photographs. *International Journal of Remote Sensing*, **26**, pp. 823–832.

TURKER, M. and SAN, B.T., 2004, Detection of collapsed buildings caused by the 1999 Izmit, Turkey earthquake through digital analysis of post-event aerial photographs. *International Journal of Remote Sensing*, **25**, pp. 4701–4714.

TURKER, M. and SUMER, E., 2008, Building-based damage detection due to earthquake using the watershed segmentation of the post-event aerial images. *International Journal of Remote Sensing*, **29**, pp. 3073–3089.